Inorganic Chemistry
Cite This: Inorg. Chem. 2018, 57, 5083−5088
Article
pubs.acs.org/IC

The Nature of Bonding in Bulk Tellurium Composed of One-Dimensional Helical Chains

Seho Yi,[†] Zhili Zhu,[‡] Xiaolin Cai,[‡] Yu Jia,*[,‡,§] and Jun-Hyung Cho*[,†]

[†]Department of Physics, Research Institute for Natural Science, and HYU-HPSTAR-CIS High Pressure Research Center, Hanyang University, 222 Wangsimni-ro, Seongdong-Ku, Seoul 04763, Korea

[‡]International Laboratory for Quantum Functional Materials of Henan, and School of Physics and Engineering, Zhengzhou University, Zhengzhou 450001, People's Republic of China

[§]Key Laboratory for Special Functional Materials of Ministry of Education, and School of Physics and Electronics, Henan University, Kaifeng 475004, People's Republic of China

ABSTRACT: Bulk tellurium (Te) is composed of one-dimensional (1D) helical chains which have been considered to be coupled by van der Waals (vdW) interactions. However, on the basis of first-principles density functional theory calculations, we here propose a different bonding nature between neighboring chains: i.e., helical chains made of normal covalent bonds are connected together by coordinate covalent bonds. It is revealed that the lone pairs of electrons of Te atoms participate in forming coordinate covalent bonds between neighboring chains, where each Te atom behaves as both an electron donor to neighboring chains and an electron acceptor from neighboring chains. This ligand−metal-like bonding nature in bulk Te results in the same order of bulk moduli along the directions parallel and perpendicular to the chains, contrasting with the large anisotropy of bulk moduli in vdW crystals. We further find that the electron effective masses parallel and perpendicular to the chains are almost the same as each other, consistent with the observed nearly isotropic electrical resistivity. It is thus demonstrated that the normal/coordinate covalent bonds parallel/perpendicular to the chains in bulk Te lead to a minor anisotropy in structural and transport properties.

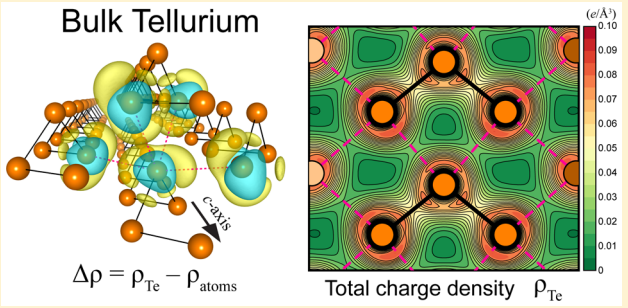

INTRODUCTION

Due to its multivalent character, tellurium (Te) exhibits a wide variety of stable structures under pressure, which contain many coordination numbers ranging from 2 to 8.[1] The most stable structure of Te has a trigonal crystal lattice at ambient pressure,[1a] which consists of 1D helical chains with a coordination number of 2. For this bulk-Te structure, the general consensus is that the nearest-neighboring atoms along the chains are linked through strong covalent bonds, while the next-nearest-neighboring atoms between the chains are coupled by weak van der Waals (vdW) interactions[2] (see Figure 1). This anisotropic bonding nature in bulk Te is naturally expected to exhibit drastically different electrical transport properties along the directions parallel and perpendicular to the chains. However, surprisingly, earlier experimental studies[3] reported that the electrical resistivity of bulk Te measured at room temperature was $\rho_{\parallel}$ = 0.26 Ω cm and $\rho_{\perp}$= 0.51 Ω cm parallel and perpendicular to the chains, respectively. Recently, these somewhat isotropic transport behaviors in bulk Te were also observed in large-area, high-quality 2D tellurium, where the ratio $\rho_{\perp}/\rho_{\parallel}$ is only ∼1.13.[4] It is, however, noted that the typical 2D layered materials with vdW interlayer interactions, such as graphite and MoS_2, exhibit a huge anisotropic behavior with $\rho_{\perp}/\rho_{\parallel} \approx 0.001$,[5] where $\rho_{\perp}$ ($\rho_{\parallel}$) represents the electrical resistivity across (along) the layers. This result indicates that the transport along the weakly vdW bound direction is

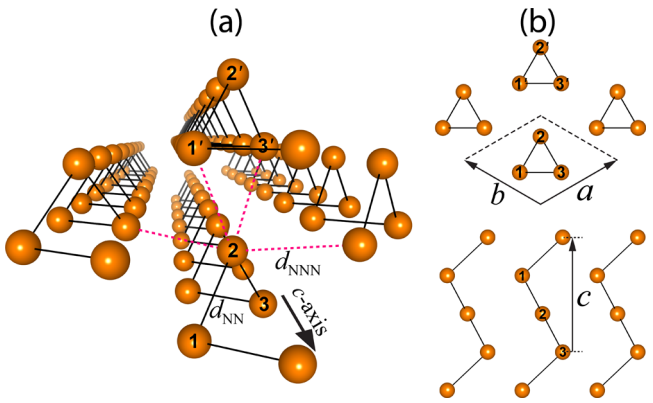

Figure 1. (a) Perspective and (b) top (upper panel), and side (lower panel) views of the equilibrium structure of bulk Te, obtained using the meta-GGA functional of SCAN. The lattice parameters are represented by *a*, *b*, and *c*.

Received: January 16, 2018
Published: April 26, 2018

DOI: 10.1021/acs.inorgchem.7b03244
Inorg. Chem. 2018, 57, 5083−5088

significantly slower than that along the chemical bond direction. Thus, the observed nearly isotropic transport properties of bulk Te in the directions parallel and perpendicular to the chains are unlikely to represent a 1D vdW crystal generally accepted so far.[2−4,6] Indeed, the extended X-ray absorption fine structure experiment[7] for the isolated selenium−tellurium (Se−Te) mixed chains confined in the channels of mordenite as well as the trigonal and amorphous Se−Te mixtures showed that the bond length between Se atoms of an isolated Se chain is shorter than that of the trigonal crystal Se and that the distance between the next-nearest neighbors in adjacent chains is smaller than twice the van der Waals radius of a Se atom. Therefore, it was not only pointed out that the coupling between adjacent chains would influence the covalent bond along the chain but also suggested that the interchain interaction might be associated with a hybridization between the lone-pair orbitals of Se atoms and the antibonding orbitals of nearest-neighboring atoms in adjacent chains. We note that the electronic structure of bulk Te has been explored using various theoretical schemes such as the tight-binding model,[2] empirical pseudopotential method,[8] and density functional theory.[9] In this paper, using systematic DFT calculations with the local, semilocal, and meta-semilocal exchange-correlation functionals, we demonstrate that the interaction between neighboring helical chains is characterized by coordinate covalent binding with lone-pair electrons, therefore enabling each Te atom to attain four coordinate covalent bonds between neighboring chains (see Figure 1). As a result, the electron effective masses parallel and perpendicular to the chains are found to be very similar at ∼0.11 m_0 and ∼0.13 m_0, respectively. Thus, our findings not only demonstrate the bonding nature in bulk Te in terms of a coordinate covalent bonding between the helical chains but also provide an explanation for the observed isotropic transport behaviors.

COMPUTATIONAL DETAILS

Our DFT calculations were performed using the Vienna ab initio simulation package (VASP) code with the projector augmented wave method.[10] For the treatment of exchange-correlation energy, we employed various functionals including the local density approximation (LDA) functional of Ceperley−Alder (CA),[11] the generalized-gradient approximation (GGA) functional of Perdew−Burke−Ernzerhof (PBE),[12] and the recently proposed strongly constrained and appropriately normed meta-GGA (meta-GGA-SCAN) functional.[13] It is known that the meta-GGA-SCAN functional improves significantly over LDA and GGA for geometries and energies of diversely bonded materials, including covalent, metallic, ionic, hydrogen, and van der Waals bonds, because it not only accurately describes the electron-correlation hole around a delocalized electron but also properly corrects the self-interaction error. A plane wave basis was employed with a kinetic energy cutoff ($E_{cut} = \hbar^2 G_{MAX}^2/2m$) of 500 eV. To calculate the charge density, we accommodated its Fourier components within a cutoff of $2G_{MAX}$. The k-space integration was done with the 25 × 25 × 19 meshes in the Brillouin zone. All atoms were allowed to relax along the calculated forces until all the residual force components were less than 0.001 eV/Å. In order to properly predict the measured band gap, we performed the hybrid DFT calculation with the HSE functional,[14] where the gap size depends on the magnitude of α controlling the amount of exact Fock exchange energy.[15]

RESULTS AND DISCUSSION

We performed a systematic study of the structural properties of bulk Te with respect to various exchange-correlation functionals. The calculated results for the total energy E_{Te} of bulk Te as a function of volume V using LDA-CA, GGA-PBE, and meta-GGA-SCAN functionals are given in Figure 2. Here, the

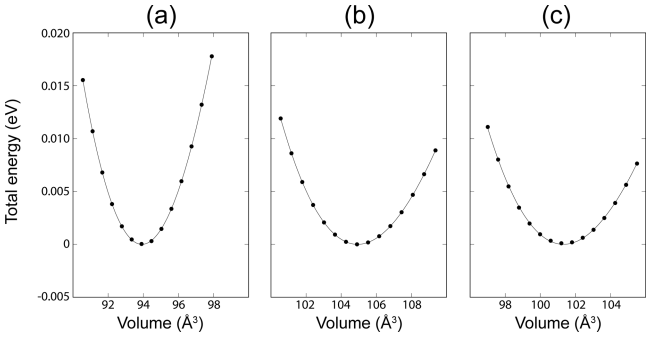

Figure 2. Calculated total energy as a function of volume using (a) LDA-CA, (b) GGA-PBE, and (c) meta-GGA-SCAN functionals.

minimum energy for each volume is determined by optimizing the axial ratio a/c and all internal atomic positions. The calculated $E_{Te}-V$ curve is fitted to the Birch−Murnaghan equation of state[16]

$$E(V) = E_0 + \frac{9V_0B}{16}\left\{\left[\left(\frac{V_0}{V}\right)^{2/3} - 1\right]^3 B' + \left[\left(\frac{V_0}{V}\right)^{2/3} - 1\right]^2\left[6 - 4\left(\frac{V_0}{V}\right)^{2/3}\right]\right\} \quad (1)$$

Therefore, we obtain the equilibrium volume V_0 and bulk modulus B, from which the equilibrium lattice constants a_0 and c_0 are evaluated. The results are summarized in Table 1

Table 1. Calculated Lattice Constants and Bulk Moduli of Bulk Te, in Comparison with the Experimental Values[a]

	a	c	d_{NN}	d_{NNN}	B (GPa)	V (Å³)
LDA-CA	4.28	5.93	2.91	3.31	38	93.9
GGA-PBE	4.51	5.96	2.89	3.50	18	104.9
meta-GGA-SCAN	4.45	5.93	2.87	3.45	18	101.2
exptl[14]	4.45	5.93	2.83	3.49	19	101.7

[a]The calculated bond length d_{NN} (d_{NNN}) between nearest neighbors (next-nearest neighbors) is also given in Å.

together with the bond lengths. It is found that LDA-CA (GGA-PBE) underestimates (overestimates) the equilibrium lattice constant a_0 in comparison to the experimental value[17] by 3.8% (1.3%), while the meta-GGA-SCAN value is in good agreement with experiment. Meanwhile, the equilibrium lattice constant c_0 is reasonably well predicted by all of the exchange-correlation functionals. Hereafter, we use the meta-GGA-SCAN functional to investigate the bonding nature of bulk Te. It is noted that the inclusion of spin−orbit coupling in meta-GGA-SCAN decreases (increases) the lattice constant a_0 (c_0) only by less than 0.02% (0.4%). Figure 1 shows the equilibrium structure of bulk Te obtained using meta-GGA-SCAN. There are two nearest neighbors (NNs) along the chain and four next-nearest neighbors (NNNs) between the chains, giving rise to a coordination number of 6. The calculated bond lengths between NNs (d_{NN}) are 2.91, 2.89, and 2.87 Å for LDA-CA, GGA-PBE, and meta-GGA-SCAN, respectively, while bond lengths between NNNs (d_{NNN}) 3.31, 3.50, and 3.45 Å. Thus,

DOI: 10.1021/acs.inorgchem.7b03244
Inorg. Chem. 2018, 57, 5083−5088

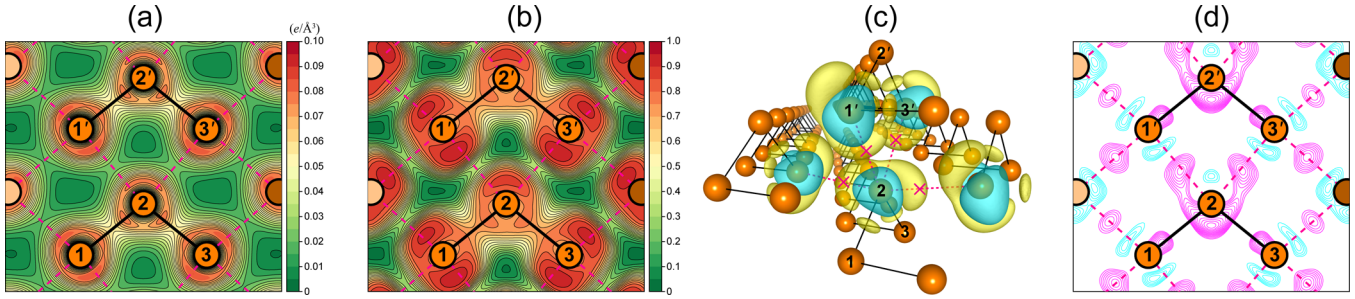

Figure 3. (a) Total charge density ρ_{Te} and (b) electron localization function of bulk Te and the charge density differences (c) $\Delta\rho$ and (d) $\Delta\rho'$, defined in the text. In (a), the first line is drawn at 5×10^{-5} e/Å^3 and the contour spacing is 5×10^{-3} e/Å^3. In (b), the first line is drawn at 0.01 and the contour spacing is 0.05. Low (high) values of ELF are shown in green (red), respectively. In (c), $\Delta\rho$ is drawn with an isosurface of $\pm 5 \times 10^{-3}$ e/Å^3. Here, the accumulated (depleted) electrons are represented by the yellow (blue) isosurface, and lone pairs of the Te(2) atom and its NNNs (Te(1′) and Te(3′)) are marked ×. In (d), the accumulated (depleted) electrons are represented by the magenta (cyan) lines, where the first line is drawn at 1.5×10^{-3} (-1.5×10^{-3}) e/Å^3 and the contour spacing is 2.5×10^{-4} (-2.5×10^{-4}) e/Å^3.

meta-GGA-SCAN reproduces well the experimental data[17] of lattice constants, bulk moduli, and bond lengths (see Table 1).

Since the magnitude of d_{NNN} is close to the interlayer distance in the typical 2D vdW materials (e.g., 3.34 Å in graphite[18] and 3.49 Å in MoS_2[19]), it has been presumed that the interchain interaction in bulk Te would be of vdW type.[2−4,6] However, it is noticeable that the sum of the vdW radii of two Te atoms amounts to ∼4.12 Å,[20] sufficiently larger than our calculated values of d_{NNN}. As discussed below, the relatively longer bond length of d_{NNN} in comparison to d_{NN} is attributed to the relatively weaker coordinate covalent bonding character between neighboring chains rather than the normal covalent bonding along the chains.

Figure 3a shows the total charge density ρ_{Te} of bulk Te, obtained using meta-GGA-SCAN. Obviously, it is seen that ρ_{Te} represents not only the covalent character for the NN bonds along the helical chains but also the relatively weaker covalent character for the NNN bonds between the chains. Note that each bond has a saddle point of charge density at its midpoint (see Figure 3a), similar to the C−C covalent bond in diamond.[21] Here, the charge densities at the midpoints of the NN and NNN bonds are 0.06 and 0.02 e/Å^3, respectively. These covalent and saddle-point characters for the NN and NNN bonds are well represented by the electron localization function[22] (see Figure 3b). To explore the more-detailed bonding character of bulk Te, we calculate the charge density difference, defined as $\Delta\rho = \rho_{Te} - \sum_i \rho_{atom,i}$, where the second term represents the superposition of the charge densities of isolated Te atoms. As shown in Figure 3c, $\Delta\rho$ shows not only a charge accumulation in the middle of the NN bond but also the presence of two lone pairs for each Te atom, while accompanying a depletion of charge in some regions around Te atoms. Such negative and positive charge redistributions around Te atoms are quite comparable to the negative and positive potential sites in the σ holes of heavy p-block elements,[23] respectively. In this sense, the nature of binding between neighboring helical chains in bulk Te can be similar to σ-hole interactions. We also note that the important role of two lone pairs in the interchain interaction was pointed out in previous theoretical and experimental works.[7,8,24]

It is thus likely that an NN bond along the chains can be characterized as a normal covalent bond but an NNN bond between the chains as a coordinate covalent bond where each lone pair of electrons participates in forming a bond with the Te atom in a neighboring chain. These two different bonding natures between NNs and NNNs are well represented by the calculated bond lengths: i.e., d_{NNN} is longer than d_{NN} by 0.4−0.6 Å (see Table 1) due to its weak coordinate covalent bonding. Here, Te tends to have the dual characteristics of both a nonmetal and a metal with ligand−metal-like bonding. Interestingly, such unique bonding features of Te can be seen in Figure 3c: i.e., the Te(2) atom with two lone pairs behaves as an electron donor to NNNs as well as an electron acceptor from NNNs (Te(1′) and Te(3′)).

To estimate the strength of the interaction between the helical chains in bulk Te, we calculate the interchain binding energy, defined by $E_b = E_{chain} - E_{Te}$, where E_{chain} is the total energy of an isolated helical chain. Here, the isolated chain is simulated using a $3 \times 3 \times 1$ supercell which separates adjacent chains by ∼12 Å. We find that LDA-CA (GGA-PBE) gives E_b = 0.490 (0.173) eV/atom, which is larger (smaller) than that (0.255 eV/atom) obtained using meta-GGA-SCAN. This overestimation (underestimation) of E_b in LDA-CA (GGA-PBE) is well represented among the calculated values of d_{NNN}, which are on the order of GGA-PBE (3.50 Å) > meta-GGA-SCAN (3.45 Å) > LDA-CA (3.31 Å). It is noted that our calculated meta-GGA-SCAN interchain binding energy of bulk Te is much larger than the observed interlayer binding energy of graphite[25] ranging between 0.031 and 0.052 eV/atom. Moreover, the bonding natures between bulk Te and such common vdW materials should be distinguished from each other. As shown in Figure 3d, the covalent bonding character between neighboring Te chains can be seen from the charge density difference $\Delta\rho' = \rho_{Te} - \sum_i \rho_{chain,i}$, where the second term represents the superposition of the charge densities of isolated chains. Here, $\Delta\rho'$ clearly shows charge accumulation in the middle regions between the chains, not supporting vdW interactions between the helical chains. We note that LDA-CA, GGA-PBE, and HSE give similar features in the total charge density and charge density differences $\Delta\rho$ and $\Delta\rho'$: i.e., the covalent character for the NN and NNN bonds, the saddle-point character of charge density at the midpoint of each bond, and the presence of two lone pairs for each Te atom.

Next, we study the elastic properties of bulk Te, which can reflect the proposed covalent bonding nature. Figure 4 shows the variation of E_{Te} as a function of the lattice parameter ratios a/a_0 and c/c_0, obtained using meta-GGA-SCAN, which predicts well the experimentally measured lattice constants (see Table 1). By using the Birch−Murnaghan equation of state, we fit the E_{Te} vs a (c) curve to obtain a bulk modulus of 18 (65) Pa. The somewhat larger bulk modulus along the c axis in comparison to the a axis indicates that the normal covalent bonding parallel

DOI: 10.1021/acs.inorgchem.7b03244
Inorg. Chem. 2018, 57, 5083−5088

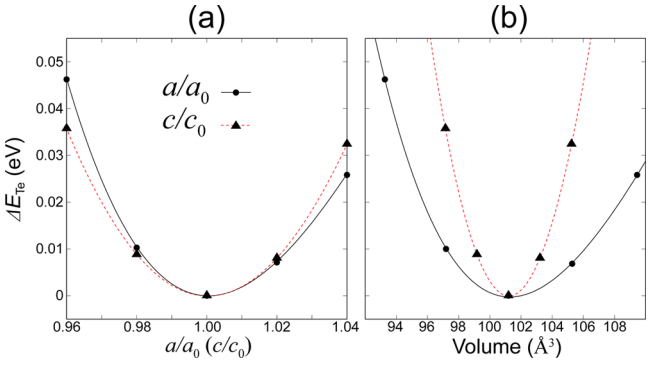

Figure 4. (a) Total energy difference (in eV per Te atom) as a function of the lattice parameter ratios, a/a_0 and c/c_0, obtained using meta-GGA-SCAN and (b) ΔE_{Te} vs a/a_0 (c/c_0) converted to ΔE_{Te} vs volume V. Here, V is equal to $\sqrt{3}a^2c_0/2$ ($\sqrt{3}a_0^2c/2$) in the direction perpendicular (parallel) to the chains.

to the chains is relatively stiffer with a change in the lattice parameter c, in comparison to the case of the coordinate covalent bonding perpendicular to the chains. However, since the two bulk moduli B_a and B_c perpendicular and parallel to the chains are of the same order of magnitude, we can say that the elastic anisotropy of bulk Te is minor, contrasting with the typical 2D vdW materials such as graphite, where the bulk moduli along the in-plane and out-of-plane directions were observed to be anisotropic with a large ratio of ~35.[26] Thus, the small ratio $B_c/B_a \approx 3.6$ in bulk Te also does not support a vdW bonding picture between the helical chains.

To further estimate the stiffness of bulk Te against the external strain, we calculate the elastic constants.[27] The bulk Te has trigonal-trapezoidal point symmetry with 32 point symmetry in the Hermann−Mauguin notation.[28] It is noted that crystals of the rhombohedral class (including trigonal-trapezoidal point symmetry) have the six independent elastic constants C_{11}, C_{12}, C_{13}, C_{14}, C_{33}, and C_{44}.[29] Moreover, the other elastic parameters such as bulk modulus (B), shear modulus (G), Young modulus (E), and Poisson ratio (ν) can be calculated.[30] Our results for C_{ij}, G, E, and ν are given in Table 2. It is seen that the present values of C_{ij} are in good agreement with previous theoretical[9b] and experimental[31] data.

Table 2. Calculated Elastic Constants C_{ij}, Shear Moduli G, Young Moduli E, and Poisson Ratios ν Using meta-GGA-SCAN, in Comparison with Previous GGA-PBE Calculations and Experiments[a]

	C_{11}	C_{12}	C_{13}	C_{14}	C_{33}	C_{44}	G	E	ν
meta-GGA-SCAN	28	6	19	9	69	30	16	38	0.19
GGA-PBE[9b]	29	7	20		63	29			
exptl[31]	33	8	26	12	72	31	17	41	0.22

[a]Elastic constants, shear moduli, and Young moduli are given in GPa.

Since the proposed normal/coordinate covalent bonding natures parallel/perpendicular to the chains have similar charge characteristics (see Figure 3a), it is natural to expect isotropic electrical transport properties as observed in experiments.[3,4] Figure 5 shows the band structure of bulk Te, obtained using meta-GGA-SCAN. We find a semiconducting feature with a band gap of E_g = 0.08 eV. This theoretical band gap is much underestimated in comparison to the experimental value[32] of

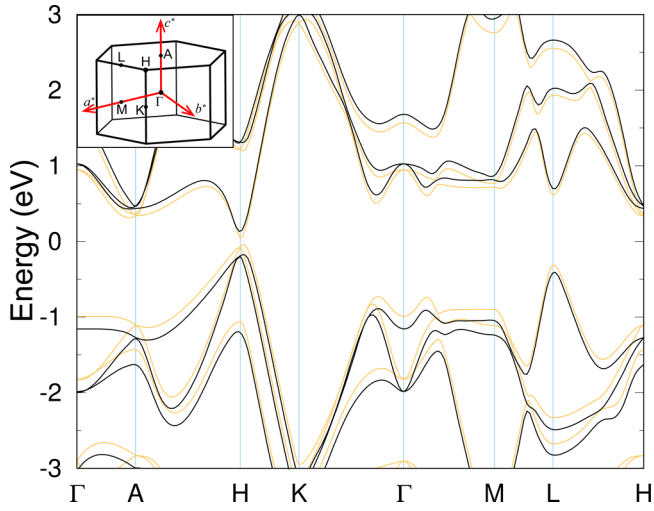

Figure 5. Calculated band structures of bulk Te using the meta-GGA-SCAN functional (bright lines) and the HSE functional with α = 0.125 (dark lines). The Brillouin zone is drawn in the inset.

0.33 eV. We find that, when the HSE functional with α = 0.125 is used, the band gap increases to E_g = 0.32 eV (see Figure 5), close to the experimental data. Meanwhile, the standard HSE calculation with α = 0.25 is found to give E_g = 0.54 eV. On the basis of the meta-GGA-SCAN (HSE with α = 0.125) band structure of bulk Te, we estimate electron effective masses parallel and perpendicular to the chains of 0.05 (0.11) m_0 and 0.11 (0.13) m_0, respectively. These results indicate very isotropic electrical transport properties of bulk Te, consistent with the measurements[3,4] of nearly isotropic resistivity parallel and perpendicular to the chains.

CONCLUSION

In summary, our first-principles DFT study of bulk Te has demonstrated that the helical chains made of normal covalent bonds are bound with each other through coordinate covalent bonds. We revealed that the coordinate covalent bonds between neighboring chains are formed by lone pairs of electrons of Te atoms. These covalent bonding characters along the directions parallel and perpendicular to the chains were found to give rise to a minor anisotropy in the structural and transport properties of bulk Te, consistent with experiments.[3,4,33] Our findings not only elucidate that the nature of binding between neighboring helical chains in bulk Te is characterized as a coordinate covalent bonding rather than the so-far accepted vdW interactions[2−4,6] but also have important implications for understanding the physical properties of Te layers, which have attracted much attention recently as a new 2D material for electronic and optical devices.[4,6b,c,34,35]

AUTHOR INFORMATION

Corresponding Authors

*E-mail for Y.J.: jiayu@zzu.edu.cn.
*E-mail for J.-H.C.: chojh@hanyang.ac.kr.

ORCID

Zhili Zhu: 0000-0002-4287-2734
Jun-Hyung Cho: 0000-0002-1785-1835

Author Contributions

J.-H.C. and Y.J. designed and supervised the work. S.Y., X.C., and Z.Z. performed the theoretical calculations. S.Y. and J.-H.C.

DOI: 10.1021/acs.inorgchem.7b03244
Inorg. Chem. 2018, 57, 5083−5088

contributed to data interpretation and presentation. S.Y., Z.Z., and J.-H.C. wrote the manuscript. All authors contributed to the scientific discussion and manuscript revisions.

Notes

The authors declare no competing financial interest.

■ ACKNOWLEDGMENTS

This work was supported by a National Research Foundation of Korea (NRF) grant funded by the Korea Government (Grant Nos. 2015M3D1A1070639 and 2016K1A4A3914691). Y.J. is supported by the National Basic Research Program of China (Grant No. 11774078). Calculations were performed by the KISTI supercomputing center through the strategic support program (KSC-2017-C3-0041) for supercomputing application research.

■ REFERENCES

(1) (a) Donohue, J. *The Structure of the Elements*; Wiley: New York, 1974. (b) Kabalkina, S. S.; Vereshchagin, L. F.; Shulenin, B. M. Phase Transition in Tellurium at High Pressures. *J. Exp. Theor. Phys.* **1963**, *45*, 2073. (c) Jamieson, J. C.; McWhan, D. B. Crystal Structure of Tellurium at High Pressures. *J. Chem. Phys.* **1965**, *43*, 1149. (d) Aoki, K.; Shimomura, O.; Minomura, S. Crystal Structure of the High-Pressure Phase of Tellurium. *J. Phys. Soc. Jpn.* **1980**, *48*, 551. (e) Parthasarathy, G.; Holzapfel, W. B. High-Pressure Structural Phase Transition in Tellurium. *Phys. Rev. B: Condens. Matter Mater. Phys.* **1988**, *37*, 8499.

(2) Reitz, J. R. Electronic Band Structure of Selenium and Tellurium. *Phys. Rev.* **1957**, *105*, 1233.

(3) Epstein, A. S.; Fritzsche, H.; Lark-Horovitz, K. Electrical Properties of Tellurium at the Melting Point and in the Liquid State. *Phys. Rev.* **1957**, *107*, 412.

(4) Wang, Y., et al. Large-Area Solution-Grown 2D Tellurene for Air-Stable, High-Performance Field-Effect. *arXiv*:1704.06202 2017.

(5) (a) Pierson, H. O. *Handbook of Carbon, Graphite, Diamond and Fulerenes: Properties, Processing and Applications*; Elsevier: Amsterdam, 1994; p 61. (b) Evans, B. L.; Young, P. A. Optical Absorption and Dispersion in Molybdenum Disulphide. *Proc. R. Soc. London, Ser. A* **1965**, *284*, 402.

(6) (a) von Hippel, A. Structure and Conductivity in the VIb Group of the Periodic System. *J. Chem. Phys.* **1948**, *16*, 372. (b) Wang, Q.; Safdar, M.; Xu, K.; Mirza, M.; Wang, Z.; He, J. Van der Waals Epitaxy and Photoresponse of Hexagonal Tellurium Nanoplates on Flexible Mica Sheets. *ACS Nano* **2014**, *8*, 7497. (c) Du, Y.; Qiu, G.; Wang, Y.; Si, M.; Xu, X.; Wu, W.; Ye, P. D. One-Dimensional van der Waals Material Tellurium: Raman Spectroscopy under Strain and Magneto-Transport. *Nano Lett.* **2017**, *17*, 3965.

(7) Inui, M.; Yao, M.; Endo, H. EXAFS Study on Selenium-Tellurium Mixed Chains. *J. Phys. Soc. Jpn.* **1988**, *57*, 553.

(8) Joannopoulos, J. D.; Schluter, M.; Cohen, M. L. Electronic Structure of Trigonal and Amorphous Se and Te. *Phys. Rev. B* **1975**, *11*, 2186.

(9) (a) Kirchhoff, F.; Binggeli, N.; Galli, G.; Massidda, S. Structural and Bonding Properties of Solid Tellurium from First-Principles Calculations. *Phys. Rev. B: Condens. Matter Mater. Phys.* **1994**, *50*, 9063. (b) Li, J.; Ciani, A.; Gayles, J.; Papaconstantopoulos, D. A.; Kioussis, N.; Grein, C.; Aqariden, F. Non-Orthogonal Tight-Binding Model for Tellurium and Selenium. *Philos. Mag.* **2013**, *93*, 3216.

(10) (a) Kresse, G.; Hafner, J. *Ab* initio Molecular Dynamics for Open-Shell Transition Metals. *Phys. Rev. B: Condens. Matter Mater. Phys.* **1993**, *48*, 13115. (b) Kresse, G.; Furthmller, J. Efficienty of *Ab*-initio Total Energy Calculations for Metals and Semiconductors Using a Plane-Wave Basis Set. *Comput. Mater. Sci.* **1996**, *6*, 15.

(11) Ceperley, D. M.; Alder, B. J. Ground State of the Electron Gas by a Stochastic Method. *Phys. Rev. Lett.* **1980**, *45*, 566.

(12) (a) Perdew, J. P.; Burke, K.; Ernzerhof, M. Generalized Gradient Approximation Made Simple. *Phys. Rev. Lett.* **1996**, *77*, 3865;(b) **1997**, *78*, 1396.

(13) Sun, J.; Ruzsinszky, A.; Perdew, J. P. Strongly Constrained and Appropriately Normed Semilocal Density Functional. *Phys. Rev. Lett.* **2015**, *115*, 036402.

(14) (a) Heyd, J.; Scuseria, G. E.; Ernzerhof, Z. Hybrid Functionals Based on a Screened Coulomb Potential. *J. Chem. Phys.* **2003**, *118*, 8207. (b) Krukau, A. V.; Vydrov, O. A.; Izmaylov, A. F.; Scuseria. Influence of the Exchange Screening Parameter on the Performance of Screened Hybrid Functionals. G. E. *J. Chem. Phys.* **2006**, *125*, 224106.

(15) Kim, H.-J.; Lee, J.-H.; Cho, J.-H. Antiferromagnetic Slater Insulator Phase of Na_2IrO_3. *Sci. Rep.* **2015**, *4*, 5253.

(16) Birch, F. Finite Strain Isotherm and Velocities for Single-Crystal and Polycrystalline NaCl at High Pressures and 300K. *J. Geophys. Res.* **1978**, *83*, 1257.

(17) Keller, R.; Holzapfel, W. B.; Schulz, H. Effect of Pressure on the Atom Positions in Se and Te. *Phys. Rev. B* **1977**, *16*, 4404.

(18) Baskin, Y.; Meyer, L. Lattice Constants of Graphite at Low Temperatures. *Phys. Rev.* **1955**, *100*, 544.

(19) Bronsema, K. D.; De Boer, J. L.; Jellinek, F. On the Structure of Molybdenum Diselenide and Disulfide. *Z. Anorg. Allg. Chem.* **1986**, *540*, 15.

(20) Bondi, A. van der Waals Volumes and Radii. *J. Phys. Chem.* **1964**, *68*, 441.

(21) Kaxiras, E. *Atomic and Electronic Structure of Solids*; Cambridge University Press: Cambridge, U.K., 2003; p 152.

(22) (a) Becke, A. D.; Edgecombe, K. E. A Simple Measure of Electron Localization in Atomic and Molecular Systems. *J. Chem. Phys.* **1990**, *92*, 5397. (b) Savin, A.; Jepsen, O.; Flad, J.; Andersen, O. K.; Preuss, H.; von Schnering, H. G. Electron Localization in Solid-State Structures of the Elements: the Diamond Structure. *Angew. Chem., Int. Ed. Engl.* **1992**, *31*, 187. (c) Silvi, B.; Savin, A. Classification of Chemical Bonds Based on Topological Analysis of Electron Localization Functions. *Nature* **1994**, *371*, 683.

(23) (a) Murray, J. S.; Lane, P.; Clark, T. σ-hole Bonding: Molecules Containing Group VI Atoms. *J. Mol. Model.* **2007**, *13*, 1033. (b) Politzer, P.; Murray, J. S.; Clark, T.; Resnati, G. The σ-hole Revisited. *Phys. Chem. Chem. Phys.* **2017**, *19*, 32166. (c) Gleiter, R.; Haerhauer, G.; Werz, D. B.; Rominger, F.; Bleiholder, C. From Noncovalent Chalcogen-Chalcogen Interaction to Supramolecular Aggregates: Experiments and Calculations. *Chem. Rev.* **2018**, *118*, 2010.

(24) Ohmasa, Y.; Yamamoto, I.; Yao, M.; Endo, H. Structure and Electronic Properties of Te-Se Mixtures under High Pressure. *J. Phys. Soc. Jpn.* **1995**, *64*, 4766.

(25) (a) Benedict, L. X.; Chopra, N. G.; Cohen, M. L.; Zettl, A.; Louie, S. G.; Crespi, V. H. Microscopic Determination of the Interlayer Binding Energy in Graphite. *Chem. Phys. Lett.* **1998**, *286*, 490. (b) Zacharia, R.; Ulbricht, H.; Hertel, T. Interlayer Cohesive Energy of Graphite from Thermal Desorption of Polyaromatic Hydrocarbons. *Phys. Rev. B: Condens. Matter Mater. Phys.* **2004**, *69*, 155406. (c) Liu, Z.; Liu, J. Z.; Cheng, Y.; Li, Z.; Wang, L.; Zheng, Q. Interlayer Binding Energy of Graphite: A Mesoscopic Determination from Deformation. *Phys. Rev. B: Condens. Matter Mater. Phys.* **2012**, *85*, 205418.

(26) Hanfland, H.; Beister, H.; Syassen, K. Graphite under Pressure: Equation of State and First-Order Raman. *Phys. Rev. B: Condens. Matter Mater. Phys.* **1989**, *39*, 12598.

(27) Le Page, Y.; Saxe, P. Symmetry-General Least-Squares Extraction of Elastic Coefficients from *Ab* initio Total Energy Calculations. *Phys. Rev. B: Condens. Matter Mater. Phys.* **2001**, *63*, 174103.

(28) Mauguin, C. Sur le Symbolisme des Groupes de Répétition ou de Symétrie des Assemblages Cristallins. *Z. Kristallogr. - Cryst. Mater.* **1931**, *76*, 542.

(29) Nye, J. F. *Physical Properties of Crystals*; Oxford University Press: Oxford, U.K., 1985; p 140. (b) Mouhat, F.; Coudert, F.-X. Necessary

DOI: 10.1021/acs.inorgchem.7b03244
Inorg. Chem. 2018, 57, 5083−5088

and Sufficient Elastic Stability Conditions in Various Crystal Systems. *Phys. Rev. B: Condens. Matter Mater. Phys.* **2014**, *90*, 224104.
(30) Hill, R. The Elastic Behaviour of a Crystalline Aggregate. *Proc. Phys. Soc., London, Sect. A* **1952**, *65*, 349.
(31) Royer, D.; Dieulesaint, E. Elastic and Piezoelectric Constants of Trigonal Selenium and Tellurium Crystals. *J. Appl. Phys.* **1979**, *50*, 4042.
(32) Anzin, V. B.; Eremets, M. I.; Kosichkin, Y. V.; Nadezhdinskii, A. I.; Shirokov, A. M. Measurement of the Energy Gap in Tellurium under Pressure. *Phys. Stat. Sol. A* **1977**, *42*, 385.
(33) Qiao, J.; Pan, Y.; Yang, F.; Wang, C.; Chai, Y.; Ji, W. Few-layer Tellurium: One-Dimentional-Like Layerd Elementary Semiconductor with Striking Physical Properties. *Sci. Bull.* **2018**, *63*, 159.
(34) Zhu, Z.; et al. Multivalency-Driven Formation of Te-Based Monolayer Materials: A Combined First-Principles and Experimental Study. *Phys. Rev. Lett.* **2017**, *119*, 106101.
(35) Chen, J.; Dai, Y.; Ma, Y.; Dai, X.; Ho, W.; Xie, M. Ultrathin β-Tellurium Layers Grown on Highly Oriented Pyrolytic Graphite by Molecular-Beam Epitaxy. *Nanoscale* **2017**, *9*, 15945.

DOI: 10.1021/acs.inorgchem.7b03244
Inorg. Chem. 2018, 57, 5083−5088